A Physics-Based Approach to Characterize Productivity Loss in the Haynesville Shale

Chad Jongeling[1], Jerrod Ryan[1], Christopher Ponners*[2], Dominick Wytovich[1], Joe Miller[1], Josh Jackson[1], Mark McClure[2], Garrett Fowler[2], 1. Chesapeake Energy Corporation, 2. ResFrac Corporation

Abstract

In 2023, Chesapeake Energy and ResFrac created the first-ever framework for hyper-calibration that includes time-lapse interference testing data in addition to using industry-standard data. The project aimed to develop a set of model parameters for predicting fracture and production characteristics within Chesapeake's Haynesville asset. Rate Transient Analysis (RTA) and analytical models were insufficiently detailed to explain productivity changes over time and required non-generalizable corrections. A fully coupled hydraulic fracture, reservoir, and geomechanical numerical modeling approach successfully described the observed historical production across a defined region. Data used for modeling included time-lapse interference tests, treating pressures, perforation imaging data, laboratory data, and production histories. The project was set up in three primary phases, which can be described as follows:

- Phase 1 Calibration – Initial Base Model: Stress profile calibration and parent well history match

- Phase 2 Calibration – Time-Lapse Interference Test: Measured and matched conductivity loss using Devon Quantification of Interference (DQI)

- Phase 3 Calibration – Model Validation Using Child Wells: Applied calibrated fracture and reservoir model to offsetting wells

Investigation in Phase 1 indicated that individual mechanisms for Stimulated Rock Volume (SRV) degradation could account for some of the observed production trends. However, additional investigation with Phase 2 was necessary to find the unique combination of stress and time-dependent conductivity degradation, proppant conductivity characteristics, and matrix compaction curves necessary to capture the measured conductivity loss and production responses. In Phase 3, model parameters replicating interference testing results successfully predicted the performance of adjacent pads with differing completion designs in the area of interest, establishing high confidence in model predictivity.

1. Introduction

1.1 Background

The Texas-Louisiana Salt basin containing the Haynesville and Bossier shales is the third largest natural gas resource play in the United States, with 56.2 Tcf of proved reserves as of 2021 (EIA 2022). Situated across more than 16 counties in Northeast Texas and Northwest Louisiana, the Haynesville Shale consists of "a dark, organic-rich, mudstone-marl facies with ubiquitous pyrite" (Torsch 2012). It is overlain by the Bossier Shale, followed by the Cotton Valley Sandstone, and underlain by the Smackover Limestone (in Louisiana).
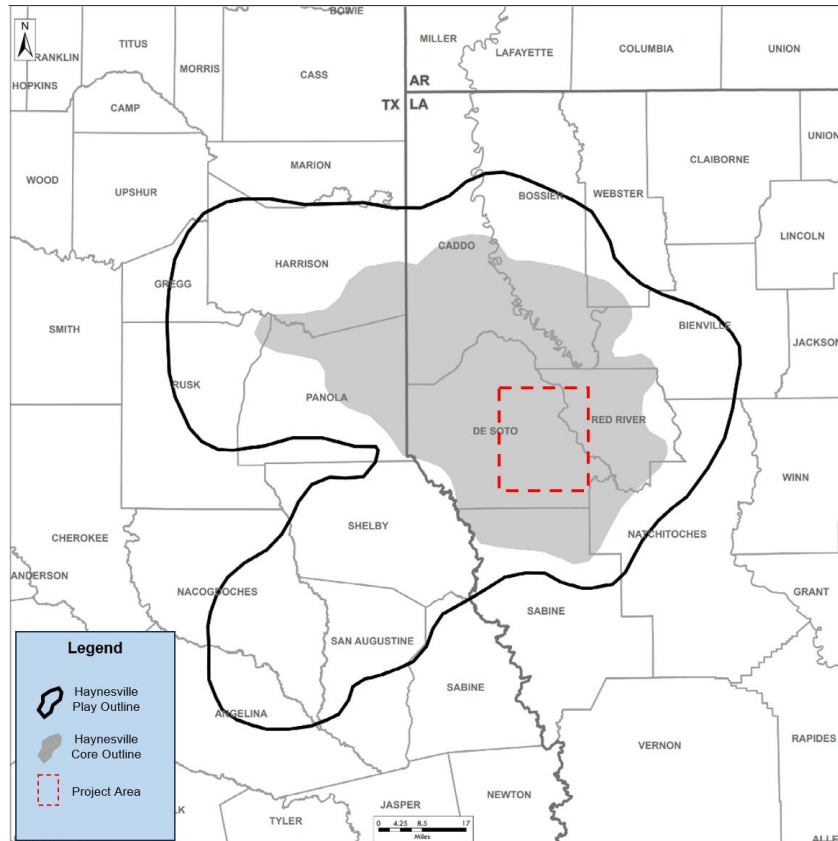

Figure 1. Haynesville Shale Basin Overview

The Haynesville is generally characterized by porosities averaging 8-12%, water saturations of 20-30%, reservoir thicknesses of 200 to 300 ft, and nanodarcy permeabilities (Torsch 2012). Unique to many shale gas plays, the Haynesville reservoirs have true vertical depths (TVD) greater than 11,000 ft and are heavily overpressured (Parker et al. 2009; Hammes et al., 2011; Thompson et al., 2010). These elevated pore pressures with gradients often greater than 0.9 psi/ft make the Haynesville particularly attractive as they enhance porosity, gas content, apparent shale brittleness, and well deliverability (Torsch 2012). Initial production rates (IPs) are greater in comparison to other shale-gas plays but also exhibit steeper first-year declines (Hammes et al., 2011).

This behavior presents a unique challenge for integrated modeling and development planning at the pad/unit scale. Various mechanisms account for the rapid decrease in well productivity. Each mechanism has different implications for the spatial distribution of depletion, leading to complexity when choosing optimal configuration and completion designs for new development wells.

In 2023, Chesapeake Energy embarked on an effort to establish new models and calibration frameworks for their Haynesville acreage. As the Haynesville asset matures, additional development frequently offsets existing producer or "parent" wells. Subsequent development offset to a parent well is defined as a "child" well. Due to this existing landscape, new projects need to consider not only the petrophysical mechanisms that cause productivity degradation but also how those mechanisms interact with child well "frac hits" on parents and preexisting parent well depletion (King et al., 2017). Previous efforts leveraging analytical modeling and RTA workflows proved difficult to match early-time and late-time trends. More importantly, correction techniques were insufficiently constrained and non-transferrable between wells of multiple vintages and/or completion designs.

For this study, we utilized a fully coupled, physics-based, 'true' hydraulic fracturing and reservoir simulator to establish a consistent set of model parameters to predict fracturing and production characteristics across the acreage position in a holistic manner (McClure et al., 2023). Time-lapsed interference tests, treating pressures, perforation imaging data, and production histories for 10 wells of various designs and vintages were leveraged to create simultaneous matches for each well. History matches honored the conductivity degradation as a function of bottom hole pressure (BHP) measured through the interpretation of the time-lapsed interference tests with the DQI method. History matches also honored the interactions between parent and child wells observed in the region.

These calibrated models helped answer questions regarding the optimization of spacing and completion design, plan stacked Haynesville and Bossier development scenarios, visualize and understand the impact of fracture geometry in the context of shrinking SRV with increased drawdown, and test the impact of depletion on child well performance.

1.2 Single Layer Numerical Model

In dry gas reservoirs, RTA techniques and numerical modeling have been acknowledged as reliable methods for characterizing well productivity; they are particularly useful for comparative assessments of well performance. However, extreme depths (TVD) and high reservoir pressures within the Haynesville and Bossier shales present unique challenges. These factors render existing simplified RTA techniques and numerical modeling less effective in fully capturing the complexity of well productivity signatures.

A common practice in simplified numerical modeling involves employing Pressure Dependent Permeability (PDP) as a principal means to account for observed declines in productivity. However, the Pressure Dependent Permeability curve has limitations in accurately representing the complete pattern of productivity decline over the well's lifecycle. As reservoir pressure decreases with production, the PDP curve suggests a corresponding decrease in permeability, leading to diminishing productivity. This curve assumes that the fundamental mechanism behind this reduction in productivity is the pressure-driven decrease in permeability. Further details on RTA will be elaborated in Section 1.4.

To mitigate the observed decrease in Stimulated Reservoir Volume (SRV), a temporary "band-aid" solution involves incorporating a negative half-length to represent the shrinking SRV (**Figure 2**). Although this method offers a means of characterization, it is inherently limited to snapshots in time and cannot accommodate the dynamic nature of reservoir behavior over time. Applying a reduction in SRV through a half-length adjustment at a singular moment is insufficient for achieving an accurate history match in simple, single-layer numerical models. Multiple adjustments are often necessary to accurately simulate the reservoir's behavior, which may lead to a history match with an improved correlation but fails to capture the underlying system dynamics. This approach also complicates understanding the relationship between the initial SRV and the percentage of degradation applied at specific times. Therefore, a more sophisticated solution is required to define the complex interplay between SRV degradation and well productivity.
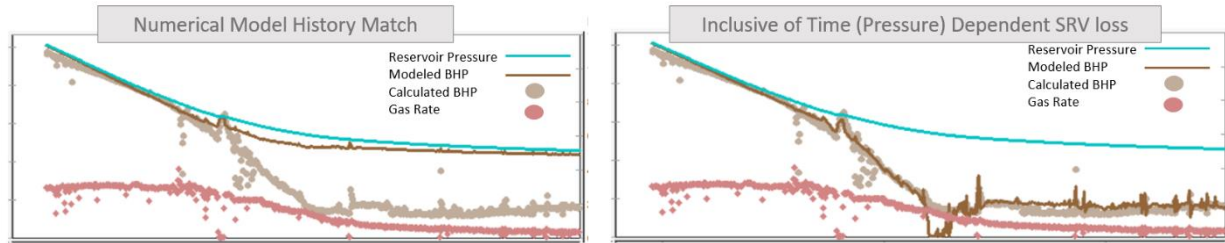
Figure 2. Example comparison of single-layer numerical models with (right) and without (left) including periodic negative half-length adjustments.

1.3 Data Availability / Calibration Techniques

Numerical modeling efforts are challenging in that the solutions generated are non-unique. While attaining a model that perfectly captures the complexities of fracture propagation and reservoir depletion is not easily achieved, the technical team sought to approach this ideal as closely as possible. This was accomplished with the incorporation of multiple constraints including standard calibration techniques included below:

- Core Calibrated Petrophysical and Geomechanical Model Utilizing the following logs
  - Gamma Ray, Resistivity, Density / Neutron, and Dipole Sonic
- Laboratory Data
  - Porosity, Water Saturation, and Permeability
  - Triaxial Core Data
  - Embedment
  - Pressure Dependent Permeability
- Fracture Driven Interactions (Frac Hits)
  - Matching observed child well pressures and impact on parent well
- Historical rates and pressures

In addition to standard techniques, the technical team focused the modeling project on an area of data abundance. It was believed that the combination of the following constraints would result in increased model uniqueness and predictivity:

- Time-Lapse Interference Testing (DQI)
- Eleven Toe DFIT tests over multiple landing zones
- Post Frac Perf Evaluation
- Variety of development styles, completion vintages, and landing horizons included in the model
  - Completion Design
  - Spacing
  - Parent / Child
  - Multiple Horizon Co-Development

The most distinctive aspect of the data utilized to refine the model was the implementation of 3 time-lapse DQI interference tests over a twelve-month period. These tests were particularly noteworthy as they provided insights into the evolution of well communication over time, shedding light on the dynamics of what was believed to be a shrinking SRV, as mentioned in Section 1.2. With this data, the team aimed to gain a deeper understanding of the mechanisms driving conductivity reduction, thereby enhancing the model's accuracy.

Additionally, the dataset included a comprehensive collection of DFIT data points, incorporating both legacy data and DFIT data obtained through Chesapeake Energy's acquisition of Vine Energy. The interpretation of eleven toe DFITs proved invaluable, offering a detailed vertical stress profile within the zone of interest. While it is customary to have representative DFITs across a field, the abundance of data in this area provided an exceptional opportunity for refined calibration of the vertical stress profile.
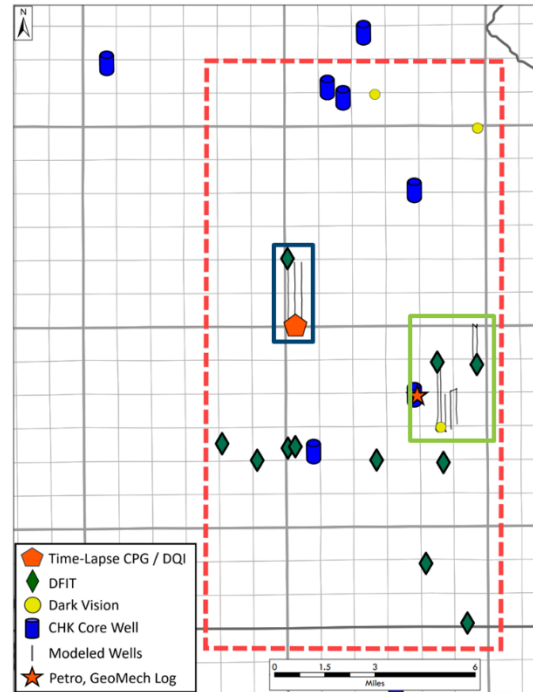

Figure 3. Regional Data Availability. As referenced in Figure 5, Phase 1 and 3 wells are outlined in green; Phase 2 wells are outlined in blue.

1.4 Physical Mechanisms for Conductivity Degradation

Rate Transient Analysis (RTA) is a common means of normalizing 'production rate versus time' trends to compare wells that may have different drawdown histories. By plotting the reciprocal productivity index on the y-axis against the square root of 'material balance time' on the x-axis (Belyadi et al., 2015; Jha and Lee, 2017), flow regime changes and/or other productivity changes due to depletion can be easily identified. Unconventional plays most commonly exhibit (at least initially) a 'linear flow' regime. On RTA plots, this flow regime is a straight line with a slope inversely proportional to $A\sqrt{k}$, effective fracture surface area and permeability. The greater the effective surface area available to flow or the permeability of the contacted area, the shallower the slope of the curve.

A generic "type" well for Haynesville gas production shows high initial rates with steep declines (Thompson et al., 2010). In the context of RTA, this behavior manifests as a short linear period with a shallow slope followed quickly by a large upward bend. Fowler et al. (2020) identifies four motifs that could potentially cause deviation from a linear flow regime and an upward bend in RTA: (a) matrix permeability, (b) fracture conductivity, (c) distance to reservoir 'boundaries,' and (d) GOR and bubble point.

For dry gas reservoirs, multiphase effects would not be applicable as only one hydrocarbon phase is present regardless of reservoir pressure. Interference between adjacent clusters in a multi-stage horizontal well also manifests as an upward curvature in RTA. While cluster interference can manifest in RTA signatures in the Haynesville, deviation from linear flow often appears to occur far earlier than estimates

from a simple radius of investigation calculation would suggest. This leaves us with permeability and fracture conductivity.

As noted in Section 1.1, the Haynesville Shale exhibits high pore pressures with minimal separation between pore pressure and the minimum horizontal principal stress (i.e., low effective stress). As pressure depletion occurs, effective stress can increase by over an order of magnitude, resulting in a reduction in permeability (Heller et al., 2014). This pressure-dependent permeability (PDP) manifests as an upward curvature in RTA; as pressure declines at the well during production, the region of reduced permeability grows with the region of pressure depletion, decreasing the effective permeability "felt" by the well. Lab data on pressure-dependent permeability for this project is discussed in Section 2.3

In an RTA context, fracture conductivity is most commonly used to match a y-intercept; finite conductivity fractures in which flow into the well is conductivity constrained will create a y-intercept greater than 0 in a plot of reciprocal productivity index (RPI) versus square-root material balance time (Fowler et al., 2020). However, if you think of the area side of $A\sqrt{k}$ as the amount of effective surface area that can be accessed at any point in time, there are several fracture and proppant characteristics that can reduce that area as a function of stress and/or time. Proppant pack conductivity naturally decreases as a function of net effective stress due to compaction and crushing. Proppant embedment physically reduces the propped area by reducing the effective proppant concentration across the fracture, particularly in areas of high-stress or relatively soft formations (Cipolla et al., 2008). Lastly, fines migration, diagenesis, or other chemical effects can reduce proppant pack conductivity as a function of time. Studies have shown that time-dependent factors have been important in matching field data in the Bakken and Permian (Pearson and Fowler, 2022).

1.5 Pressure Interference Test Interpretation

Interference testing is a relatively inexpensive means of assessing the strength of hydraulic connections between wells. In a standard pressure interference test, one or more wells are sequentially placed on production after being shut in. Changes in the pressures measured in offset well(s) can be interpreted to yield information on the connections between wells and potential interference.

The 'Devon Quantification of Interference' (DQI) method introduced by (Almasoodi et al., 2023) takes a novel approach to directly calculate the fracture conductivity between two wells in an interference test. The DQI method starts by performing a curve fit to the initial pressure response at the monitoring well. Observed from an offset position, the 1D diffusivity equation is:

$$P(y,t) - P(y,0) = \frac{2q_0\sqrt{\frac{\alpha t}{\pi}}}{K}\exp\left(-\frac{y^2}{4\alpha t}\right) - \frac{q_0 y}{K}\text{erfc}\left(\frac{y}{2\sqrt{\alpha t}}\right), \qquad (1)$$

where q_o is the production rate per fracture (in reservoir volume, not surface volume), y is the offset distance, α is the hydraulic diffusivity, and K is a lumped parameter. The measured pressure transient can be matched by varying the parameters K and α. They are defined as:

$$\alpha = \frac{k_f W}{\mu\left(\frac{dW}{dP}+c_f W\right)} = \frac{C}{\mu\left(\frac{dW}{dP}+c_f W\right)}, \qquad (2)$$

$$K = \frac{CH}{\mu}, \qquad (3)$$

where C is fracture conductivity, k_f is fracture conductivity, W is fracture aperture, c_f is the fluid compressibility, μ is the fluid viscosity, and H is the fracture height.

While matching a full pressure transient of an interference test would be complex and unpractical, the objective of the curve fit with Equation 1 is to focus solely on matching the *initial* pressure response at the monitoring well. The arrival of the pressure transient is dependent only on hydraulic diffusivity, α,

and is not affected by uncertainties in flow geometry, K, drawdown rate at the production well, or any other parameters.

Given a value of hydraulic diffusivity, the fracture conductivity can be estimated by plugging into Equation 2. When applying Equation 2, the fluid compressibility and viscosity should be estimated from the fluid in the fracture during the test. The values of fracture aperture and its derivative, W and $\frac{dW}{dP}$, can be assumed to be 0.03 inches and a range of 2e-6 to 8e-6 inches/psi, which are reasonable estimates for propped fractures (Almasoodi et al., 2023).
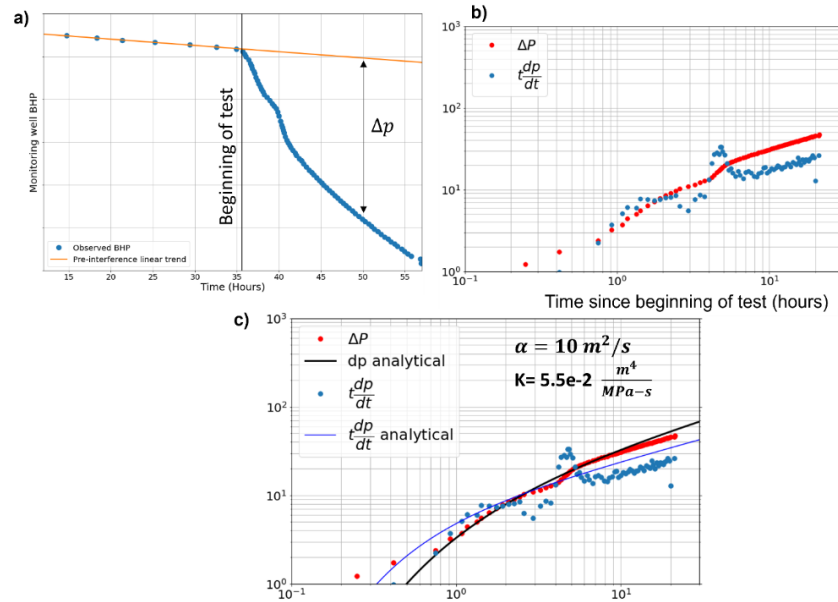

Figure 4. Example of the plots required for interpreting an interference test using the DQI method. a) Pressure observations in a monitoring well before and after an offset well is put on production. The timing of the offset well POP (Put on Production) is marked by the vertical black line, indicating the beginning of the interference test. The orange line shows the linear trend of the pressure before interference which is extrapolated to the interference test time period to calculate Δp; b) Δp and $t\frac{dp}{dt}$ observed during the interference test; c) Δp and $t\frac{dp}{dt}$ from the analytical solution (black and blue lines) are fitted to the pressure and derivative observations by a trial and approach varying α and K, to find a good fit. Reproduced from (Almasoodi et al. 2023)).

For the purposes of this project, we utilize this DQI methodology for interference test interpretation as it yields an understood physical parameter that can serve as a direct history-matching parameter in the numerical simulator.

1.6 Details on the Numerical Simulator

A fully coupled hydraulic fracturing, reservoir, and geomechanics simulator was used for this project. McClure et al. (2023) provide full details of the software. The simulator represents hydraulic fractures as true fractures, with apertures (element widths) on the order of millimeters for the entire simulation duration. Matrix elements are represented by volumetric elements in a rectilinear grid. The wells are meshed to the surface with linear elements. A specialized '1D submesh method' (McClure et al., 2023) couples these nonconforming meshes, maintaining numerical accuracy even with coarse matrix element sizes. At every time step, the simulator satisfies mass balance for all fluid components, water solutes, and proppant types. In the wellbore, momentum balance is satisfied. Fracture propagation is modeled with the MuLTipEl algorithm developed by Dontsov (2022). The code also employs complex mechanisms for proppant transport, including gravitational settling, viscous drag, proppant bridging, and the smooth transition from slurry flow through an 'open' fracture to fluid transport through a 'closed' fracture.

Several key simulator capabilities enable the realistic representation of multi-well pads, parent-child effects, and the physical mechanisms underlying well productivity degradation:

- The simulator solves the equations of linear elastic continuum mechanics to calculate stress changes caused by fracture opening and propagation and pore pressure depletion at every timestep.

- Fracture conductivity is calculated implicitly as a function of aperture, proppant concentration, and effective normal stress. Proppant concentration and proppant pack conductivity also vary with effective normal stress due to proppant embedment and compaction curves.

- Fractures are allowed to collide and/or connect dynamically with offset wells, allowing for the simulation of parent-child relationships. Special boundary conditions are used in the wellbore to allow for production and crossflow within wells during frac hits.

- Matrix compaction is modeled with isotropic or anisotropic pressure-dependent permeability, allowing for permeability loss with depletion.

2. Modelling Workflow

2.1 Project Area Overview

The study area includes 10 wells from 2011 to 2021 vintages within the same general township. Some wells were unbounded for their entire lifetime, while others experienced parent-child relationships as offset wells were drilled into areas with differing levels of depletion. Eight of the 10 wells were drilled in the Haynesville, while two were drilled in the Bossier. Additionally, stage length and completion designs varied widely within the group: cluster spacing ranged from 15ft to 60ft, fluid loading ranged from approximately 40 bbl/ft to 110 bbl/ft, and proppant loading ranged from 1,300 lbs/ft to 4,600 lbs/ft. Multiple proppant types were utilized, including 100M, 40/70 Brown, 40/70 White, and 40/140M. The wide range of designs, vintages, drawdown strategies, and depletion configurations presented a unique opportunity for a well-constrained model by simultaneously matching all wells in the area.

Figure 5 shows a map of the region with wells colored by approximate vintage. Blue wells are parent wells without any offset depletion. The red wells were drilled ~6 years after the offsetting blue well; the yellow wells were drilled ~4 years after the red wells.
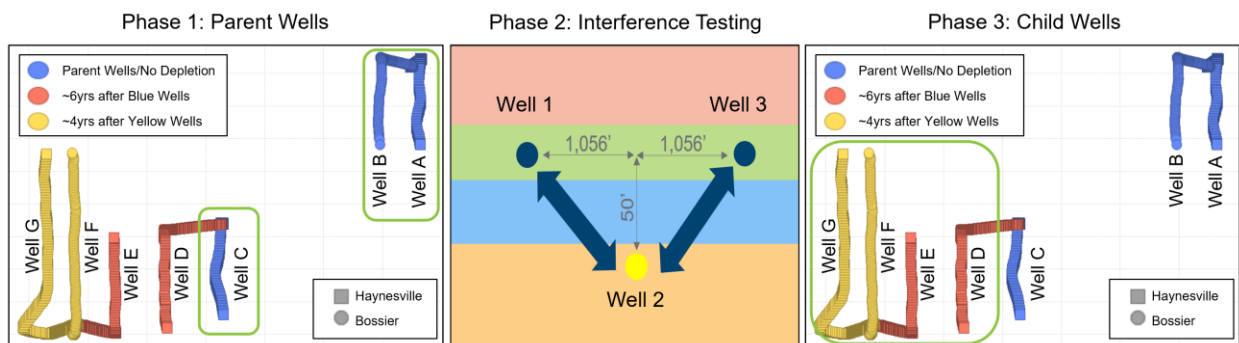

Figure 5. Overview of the core project phases. Phase 1 & 3 show map views while Phase 2 shows a gun-barrel view of the wells used for interference testing. Refer to Figure 3 for relative locations of each phase's wells.
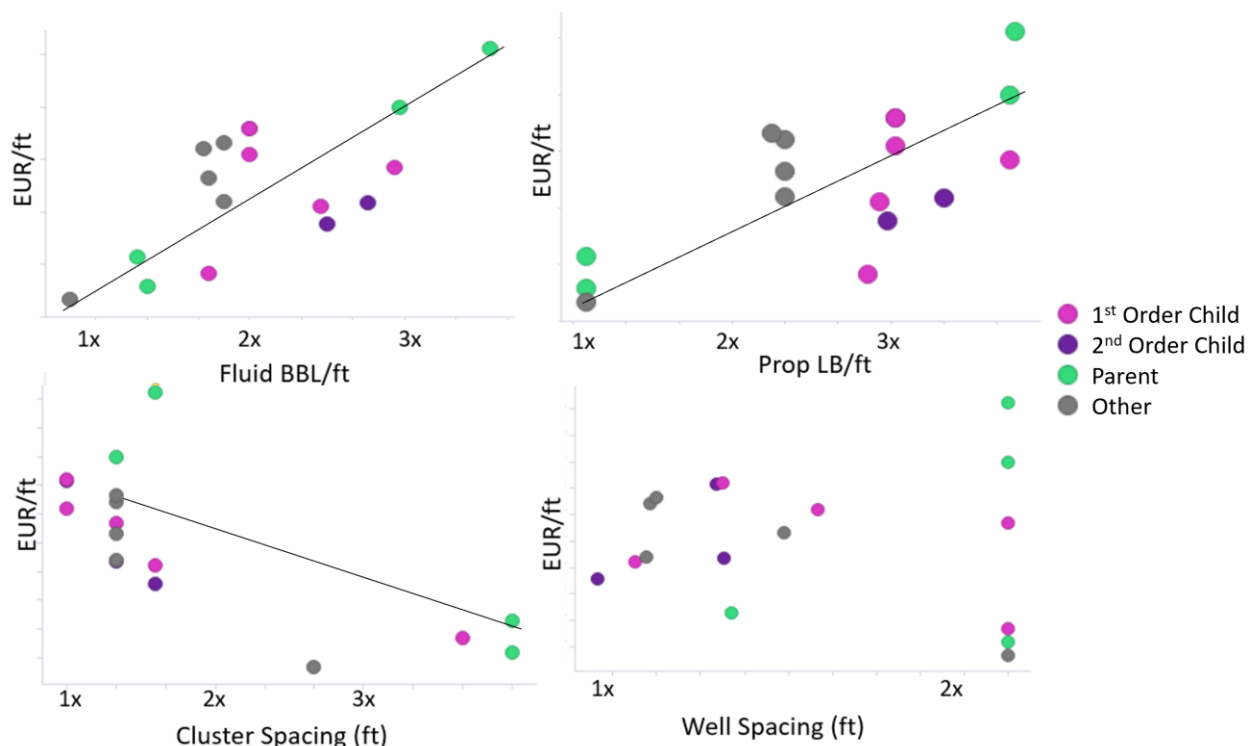
Figure 6. Correlations between completion parameters and DCA-derived gas EURs for various wells in the study area.
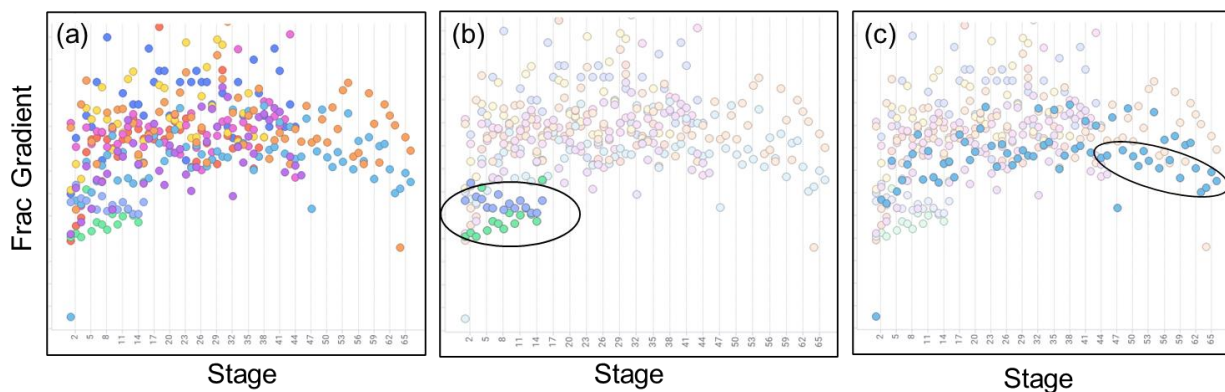

Figure 7. Initial Shut-In Pressures (ISIPs) versus stage for the wells Phase 1 and 3. Frame (a) highlights all wells. Frame (b) highlights two wells with no prior depletion but the smallest completion size and widest cluster spacing. Frame (c) highlights one well showing potential depletion effects when entering the region of a parent well.

Examining data from these 10 wells, several observations were gathered to propose hypotheses to key questions proposed at the beginning of the project—namely the explanation of damage mechanisms observed in well productivity—and to guide the modeling workflow. **Figure 6** shows correlations between projected EURs and various stage design and completion design parameters. Unsurprisingly, there is a strong correlation between completion size and EUR; completion design is a large factor in relative performance. However, there is also an indication that depletion or frac inefficiency may be playing a role as child wells are underperforming parent wells with similar completions in some situations. In addition, completion size was observed to be an influence when comparing EUR and well spacing.

Figure 7 shows Initial Shut-In Pressures (ISIPs) versus stage for all wells in the study area. From frame (a), we observe possible indication of ISIP escalation for the several initial stages in each well, indicating the potential importance of stress shadowing in fracture propagation. Frame (b) highlights two wells with the smallest completion sizes and widest cluster spacing; markedly lower ISIPs for these wells (with no prior depletion) indicate possible support for stress shadowing increasing net pressures. An indication of possible depletion from parent wells is noted in frame (c), which highlights how one of the yellow wells' ISIPs is reduced when it enters the potentially depleted zone.

In the context of productivity degradation, the synthesis of several diagnostics indicated that some mechanism(s) to explain changing well productivity was/were necessary. For example, comparing RTA responses for wells with different cluster spacing made it unlikely that inter-frac interference was the sole cause of the bend in RTA response. A comparison of the productivity index over time of wells with differing drawdown strategies made it clear that the mechanism controlling conductivity was more driven by BHP than through a time component. Lastly, 3 of the 10 wells were on a single pad with interference tests run at initial production (POP), 6 and 12 months. These tests showed a clear reduction in communication between the wells over time.

A plan was developed using these observations to allow the history-matching workflow to follow the most linear process possible. As shown in **Figure 5**, Phase 1 included the standing up of the model and a rough history match of 3 parent wells. Phase 2 would include interpreting the time-lapse interference tests and matching the observed SRV degradation in the model. Phase 3 applied the parameters matching SRV degradation to the remaining child wells in the model, refining the overall history match parameters with the observed parent-child effects. Each subsequent model calibration was reconciled with the prior model parameters to find a common parameter set. The hope was that a single set of model parameters could be arrived upon that accurately predicted fracturing and production performance across a range of well designs and developmental scenarios.
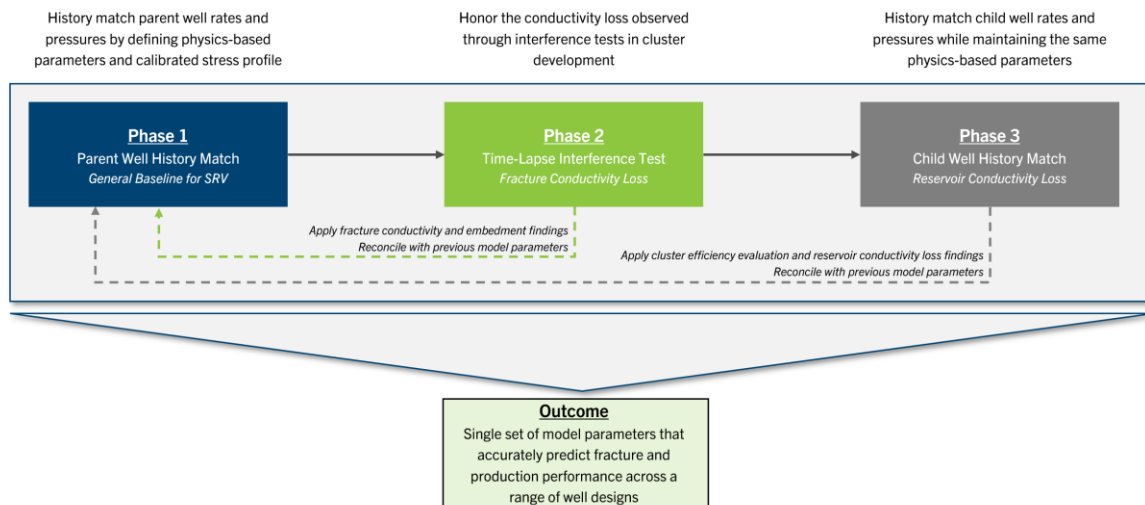

Figure 8. Summary of the full project workflow

2.2 Model and Stress Profile Construction

Modeling began with the gathering and processing of the detailed data required to accurately model the 10 wells in the project. This included well surveys, geosteering reports, well operational histories, production time series, perforating designs, treatment schedules, frac fluid rheologies, proppant specifications, black-oil models, and geologic properties. Data was continuously ingested and re-presented to all participants to ensure consistent understanding and buy-in from all disciplines.

One key pre-processing step before history matching a model in the fully-coupled hydraulic fracturing and reservoir flow paradigm utilized in this study is calibration of the stress profile. (Singh et al., 2020) shows how changes in lithology can result in changes in stress (and stress gradient) across the vertical profile. This layering of lithologies can create various degrees of height containment of fractures. While stress profiles are commonly calculated from sonic log properties using a Modified Eaton's Method (Thiercelin and Plumb, 1994; Blanton and Olson, 1999) or viscoelastic stress relaxation (VSR) method (Singh and Zoback, 2022), both methods require calibration to points of known stress.

Given the known importance of the stress profile to fracture geometries and planned multi-bench development sensitivities, much care was taken in calibrating and upscaling the stress model for the numerical simulator. Eleven DFITs from wells in the Haynesville and Bossier were analyzed and determined to be valid, resulting in the determination of stress, permeability, and pore pressure. Stress estimates were generated utilizing the 'compliance method' as described by (McClure et al. 2019). Permeability and pore pressure estimates followed the methods described by (McClure et al. 2019) following the best practices described in (Mcclure et al., 2022).

The left of **Figure 9** shows the initial stress profile with the various DFITs depth-adjusted to match the log stratigraphy. Based on the DFITs' results, we reduced the pore pressure and stress in the Bossier intervals. Additionally, we reduced the stress in one of the Haynesville benches and smoothed out the stress profile in the Gilmer and Smackover. While some adjustments were made before beginning the Phase 1 history match, several were settled upon iteratively when undergoing Step 1 of the history matching workflow outlined below.
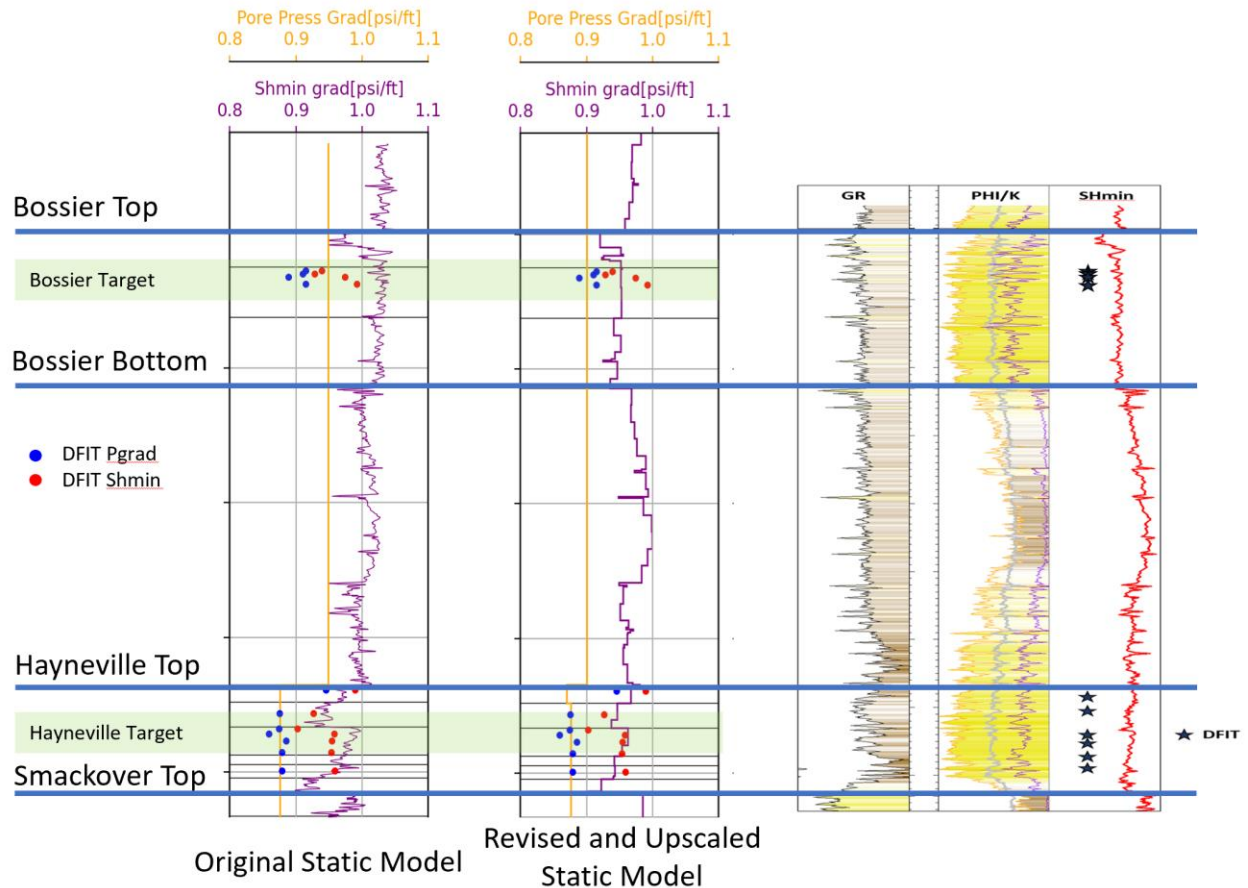

Figure 9. Comparison of the original stress and pore pressure profiles before and after calibration to regional DFITs.

2.3 Phase 1 – Parent Wells History Match

All phases of a well's lifecycle are simulated in the model, resulting in the need for all fracturing and production characteristics to be matched simultaneously. To focus this effort, the various datasets discussed in Section 2.1 were summarized into a list of 'key observations.' This list of history-matching objectives is intended to distill historical observations from multiple data sources into a singular goal that the history-matched model should exhibit. The key observations with the model parameters used to achieve a match for Wells A, B, and C are shown in **Figure 10**.

Type Calibration	Key Model Characteristics	Model Application
ISIP Escalation	ISIP escalation of 750 PSI.	Put in place external fractures with estimates of fracture size, net pressure.
Perforation efficiency	Regional perf imaging data shows cluster efficiency of 75-85% for similar cluster spacings; data of post-frac perf diameter	Erosion 'alpha' controlling erosion rate. Tensile strength to control cluster initiation.
Fracture geometry	Inferred constraints from interference tests in Phase 2 indicate a minimum fracture half-length of 600+ ft. Literature review (Younes et al. 2011) would suggest HSVL heights of 500-600 ft with more vertically concentrated growth into lower Bossier.	Toughness, Relative Fracture Toughness, Stress Profile, Pressure Dependent Permeability (leakoff)
Treating Data	ISIPs	
Treating Data	Average WHP during Treatment	Wellbore friction multiplier
Propped area geometry	Inferred constraints from interference tests in Phase 2 indicate a minimum propped half-length of 600+ ft	Maximum immobilized proppant per area
Production	Match GAS RTA Curves to create bend upward after 3000psi of depletion	Initial early time match with permeability; Negative pressure dependent permeability; Kept in mind other mechanisms: time dependent conductivity loss, stress sensitive embedment, proppant conductivity curves for Phase 2 calibration
Production	Fine tune GWR	Relative permeability curves; Fine tune flowback with water banking / water holdup

Figure 10. Phase 1 history matching key observations.

McClure et al. (2022) outlines a recommended framework for history matching in a simulator with a coupled fracturing and reservoir paradigm. A simplified general workflow is as follows:

1. Utilize any available diagnostics to constrain fracture geometries through adjustments in the stress profile, fracture toughness, and effective leak-off.

2. Match perforation efficiency through adjustments in perforation erosion and tensile strength.

3. Add external fractures to the sector model to match ISIP escalation and observed stress shadowing.

4. Calibrate wellbore friction, near-wellbore tortuosity, and viscous pressure drop inside fractures to match treating pressures and ISIPs.

5. Leverage information from interference tests to calibrate the size of the propped area.

6. Adjust bulk permeability, relative permeability curves, and pressure-dependent permeability to match production trends for all streams.

This framework aims to keep the history-matching process as linear as possible. In practice, however, there are, by necessity, many iterative cycles. For instance, steps one and five above will likely be changed during the matching of the interference tests, which may necessitate adjustments to permeability.

The details of how each model parameter outlined in Figure 10 is adjusted to obtain a model match are unnecessary in this context. (Pudugramam et al., 2022; Fowler et al., 2023; Ratcliff et al., 2022) all provide detailed discussions on using these various tuning parameters in this numerical simulator.

Highlighting one observation, **Figure 11** shows regional data on cluster efficiency gathered through perforation imaging on 5 wells; average efficiency targets are shown as stars. Cluster efficiency clearly degrades with decreasing cluster spacing. Reduced isolation between clusters combined with greater levels of stress shadowing prevents a significant number of clusters from initiating. This data was used to tune perf erosion and tensile strength parameters to create a match for Wells A, B, and C. While these wells don't include the full range of cluster spacings observed in this field data, a brief sensitivity on the Phase 1 history-matched model shows that the model is correctly capturing this effect (**Figure 11**).
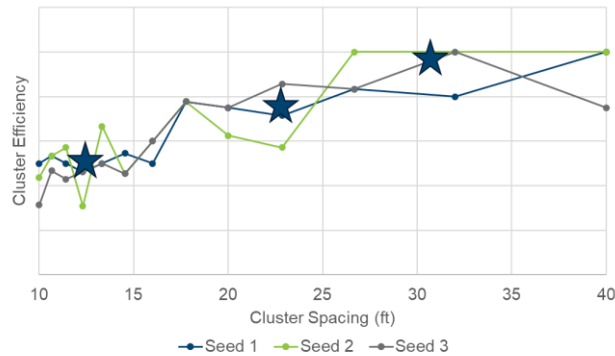

Figure 11 Cluster efficiency match in Phase 1 model with targets (stars) from regional observations. Different colors represent simulations with different random seeds to understand natural variances in the simulations.

The goal of Phase 1 was to establish a general baseline for the potential stimulated reservoir volume (SRV) accessed by the parent wells, with the knowledge that further refinement would follow. With an initial history match of unbounded parents completed, the next steps were to begin exploring the various methods that could account for the observed SRV degradation in the field.

As discussed in Section 1.4, five main physical mechanisms were identified that could decrease well productivity over time, as drawdown and net effective stress on the fractures increase. They include proppant pack conductivity, proppant pack compressibility, stress-sensitive proppant embedment, pressure-dependent permeability (matrix compaction), and time-dependent proppant conductivity loss. With several degrees of freedom due to these five parameters, a range of "bracketing" sensitivities were conducted to determine whether each factor was necessary but not sufficient, necessary and sufficient, or not necessary to match the level of productivity degradation observed in the field. In-house lab data was available for proppant pack conductivity, proppant embedment, and pressure-dependent permeability and was utilized to set the boundaries of realistic values for the sensitivities.

Figure 12, **Figure 13**, and **Figure 14**, portray the sensitivities' results for pressure-dependent permeability, proppant embedment, and time-dependent conductivity loss. The lab data (blue) and the end members of the sensitivities (gray) are also shown for pressure-dependent permeability and proppant embedment. The dotted lines in the time series plots represent the field data, while the solid lines are the model results.

Sensitivity results show each of these mechanisms, as bounded by lab data, theoretically can account for the overall magnitude of well productivity reduction. None of them individually perfectly match the observed flattening of the cumulative production curves often correlated with flowing bottom hole pressure (FBHP) reaching maximum drawdown. If taking a "yes and" approach by including each mechanism to a moderate extent, there would likely be non-uniqueness in the different combinations of

parameters to achieve a similar match. The interpretation of the interference tests in Phase 2 of the project was designed to help separate these functions and create a unique match.
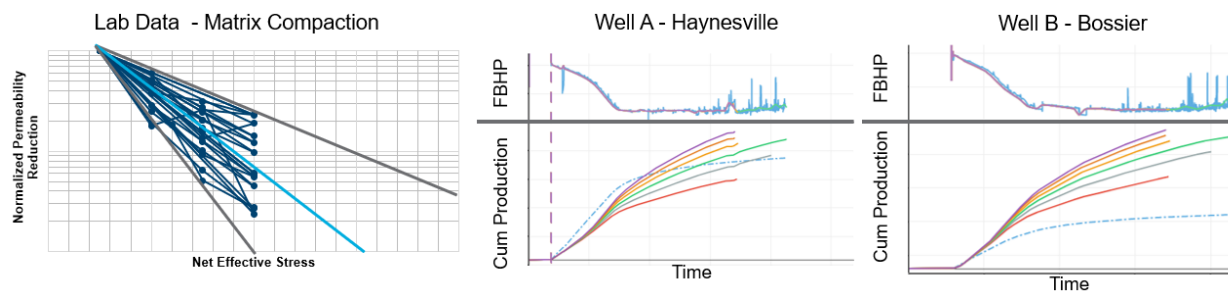

Figure 12. Left – Lab measurements of matrix compaction (negative pressure-dependent permeability). Middle and right – Pressure dependent permeability on two Phase 1 parent wells; sensitivity endpoints are bounded by gray curves from data.
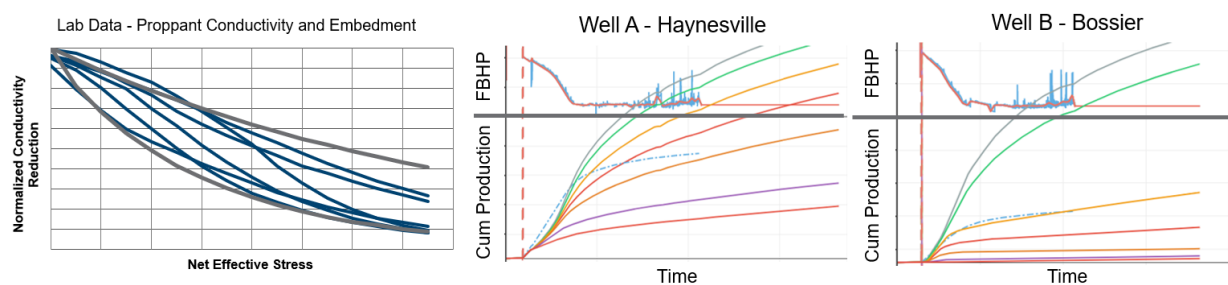

Figure 13. Left – Lab measurements of proppant conductivity and embedment. Middle and right – Embedment and proppant conductivity sensitivities on two Phase 1 parent wells; sensitivity endpoints are bounded by gray curves from data.
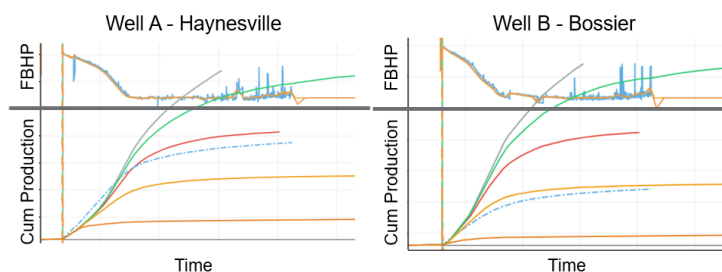

Figure 14. Time dependent conductivity loss sensitivities on two Phase 1 parent wells.

2.3 Phase 2 – Conductivity Degradation Characterization

The center of **Figure 5** shows the configuration of three wells studied as part of Phase 2 of the modeling workflows. Wells 1-3 are wine racked between two stratigraphic intervals in the Haynesville spaced at 1,056 ft apart. They are in a similar geologic setting compared to the wells used for Phase 1 and 3 and have like completion designs. Time-lapsed interference tests were conducted for this pad at 1 month, 6 months, and 12 months into production. Each time, all wells were shut in for several days, and the BHP was allowed to stabilize. Well 3 was brought back online, and the pressure response was monitored at Well 2; one day later, Well 1 was opened.

The six interference tests were analyzed using the DQI method outlined in Section 1.3 to leverage this observation more quantitatively in the numerical model. This yielded estimates of the conductivities of the pathways connecting neighboring wells. As shown in **Figure 15**, the connection strength between wells degrades substantially over time, with conductivities 50% lower six months into production and 80% lower 12 months into production relative to the well connections at one month. With data

specifically measuring fracture conductivity degradation, the effects of proppant conductivity, proppant embedment, and time-dependent conductivity loss could be separated from the reservoir effects of pressure-dependent permeability and cluster-to-cluster interference.
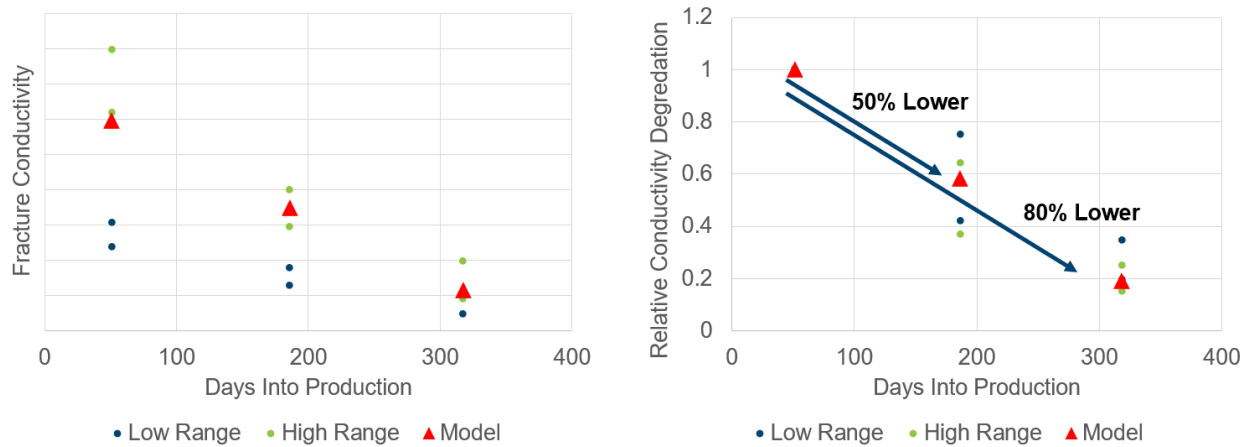

Figure 15. Results from the DQI interpretation of the 6 interference tests conducted over the first year of production for Wells 1-3.

A new model was constructed in the simulator to represent Wells 1-3, with the model parameters tuned from the Phase 1 history match. The exact timelines of the interference tests were also implemented in the simulator. This way, the DQI analysis of the interference tests in the model could be matched with field data and supported by 3D visualization.

The intent of this workflow was to start with the most simple, necessary, and physically plausible mechanisms first and add complexity as necessary. The general matching workflow was as follows:

1. Start with the average values from lab data on pressure-dependent permeability, proppant conductivity, and embedment. Increase fracture size and propped area until visual confirmation of fracture connections and proppant bridging between wells is observed. In the simulator, this was accomplished through a reduction in 'relative fracture toughness' and 'maximum immobilized proppant'. The propped area was calibrated such that the tips of the proppant pack just barely overlapped.

2. Adjust proppant 'k0' (the scaling factor for proppant conductivity at zero effective normal stress) until the conductivity of the first test is matched. The 'best-fit' k0 was just below the mid-point supported by the spread of lab data.

3. If necessary, adjust the proppant pack compressibility to match six and twelve-month tests.

4. If necessary, adjust the level of stress-sensitive embedment to match six and twelve-month tests. Steps three and four were ultimately calibrated simultaneously. Proppant pack compressibility alone could match Test 2 well, but not simultaneously with Test 3. Combining the two parameters around the midpoints supported by lab data yielded the best match. **Figure 16** shows an example of a single-variable sensitivity on stress-sensitive embedment, showing the increased level of conductivity degradation with increasing embedment.

5. If necessary, add time-dependent conductivity loss to match six and twelve-month tests. Ultimately, this parameter wasn't necessary to match the interference test data, but the option remained open to add it in Phase 3 of the modeling workflow to further tune EURs if necessary.
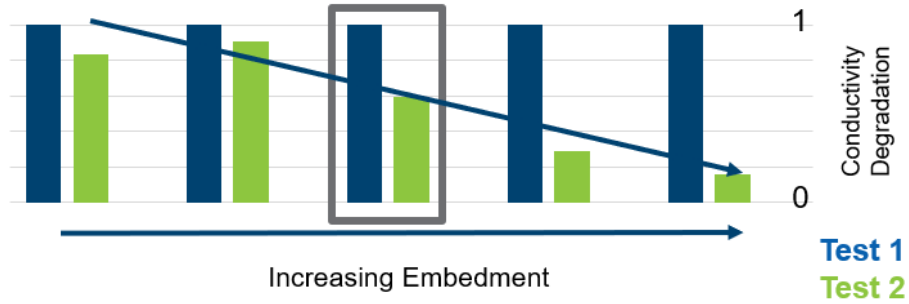
Figure 16. Example of conductivity degradation as a function of increasing embedment.

The 3D results of this interference calibration process area are shown in **Figure 17**. For each test, the screenshot is taken roughly three hours after the POP of Well 3, but before the POP of Well 2. The first column shows the interference test with varying pressures as the tests were taken at different times in the wells' life. In the middle column, the propped areas between each well just barely overlap. While the size of this proppant cloud doesn't change significantly over time, the fracture conductivity shown in the right column does degrade over time; the red circles indicate this in
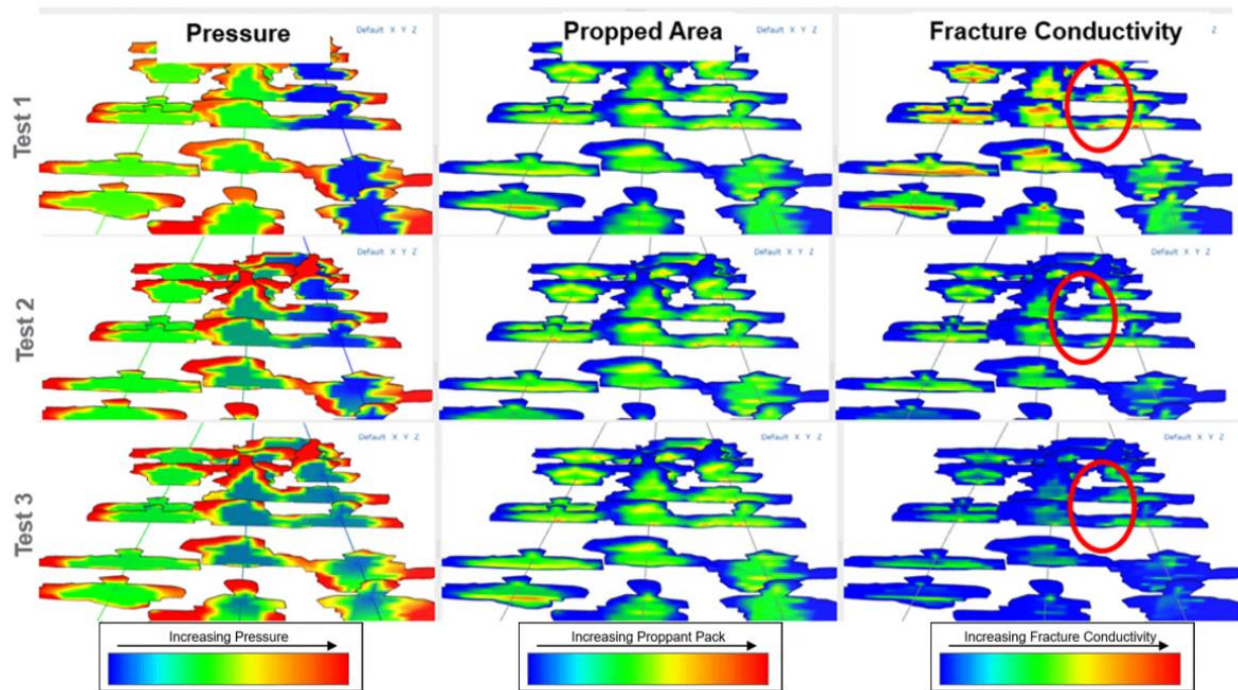
Figure 17. Due to proppant pack compressibility and embedment, the number and strength of the conductive pathways between wells are reduced over time until there are only weak connections by test three. This is a visual confirmation of the DQI tests through time.

The red triangles in **Figure 15** show the DQI calculated conductivities from the calibrated model compared with those calculated from the field data. There is a satisfactory match.
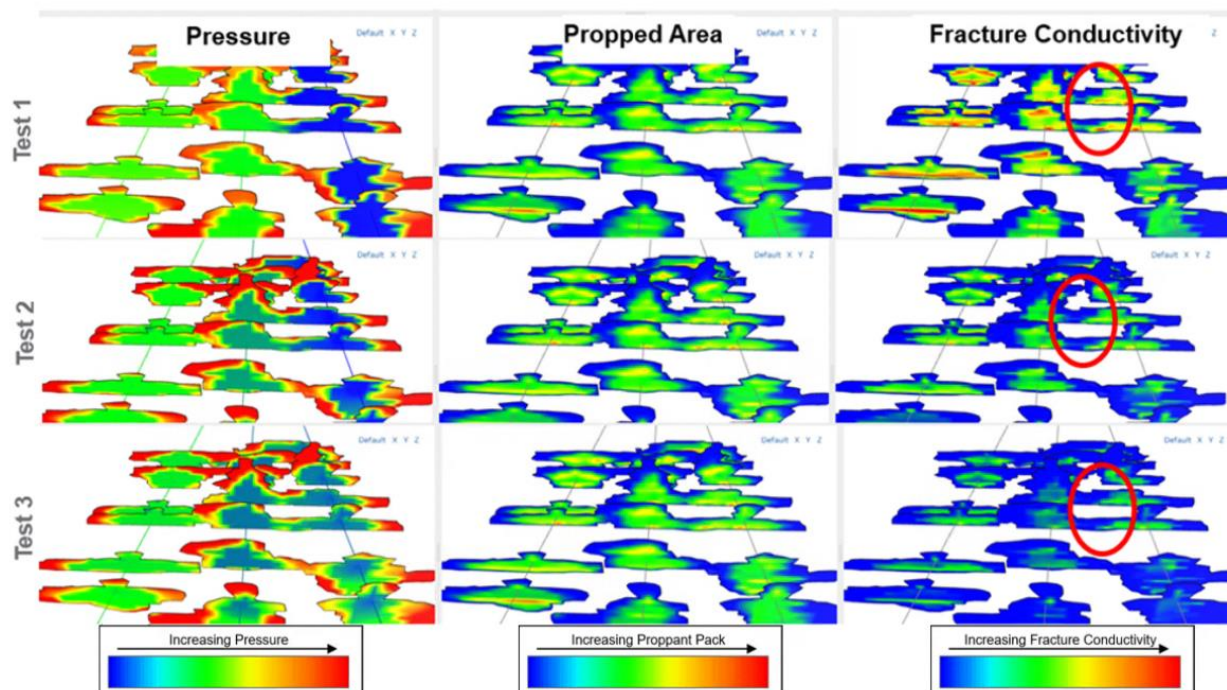
Figure 17. Visualization of Well 1-3 fracture geometries after interference test conductivity loss calibration. Each test is shown right after the POP of Well 3 (right) before the POP of Well 2.

2.4 Phase 3 – Child Wells History Match

Calibration from pressure interference tests provided confidence in the size of propped and unpropped fracture networks and an understanding of how SRV may shrink over time as net effective stress increases. Leveraging this information any remaining bend in the RTA curves can be attributed to reservoir effects.

The parameters from this 'conductivity history match' were applied to the model with Wells A and B and to the extended Well C model, now including Wells D, E, F, and G. This new model included all well histories for the three vintages, including differing frac jobs, completion designs, and stage lengths. Boundary controls included all shut-ins and pre-loads applicable to the multiple generations of parent-child wells.

Step 6 of the history matching process outlined in Section 2.3 was repeated for all 7 wells concurrently. Automated history matching workflows were run to simultaneously adjust permeability, relative permeability curves, negative pressure dependent perm (bounded by lab data), water banking, and parameters to best match the production series for the 7 wells. No additional adjustments to fracture geometries nor propped areas were made. The resulting production history matches are shown in **Figure 18** and **Figure 19**.

The wells modeled in this region had a variety of completion designs, parent-child configurations, and Haynesville / Bossier co-development, as shown in **Figure 5** and **Figure 6**. The simultaneous match of all these wells with a singular model parameter set yielded confidence in the model's predictive capabilities. Additionally, the workflow characterization of the dynamic fracture conductivities through interference testing provided confidence in a unique solution without excessive overfitting.
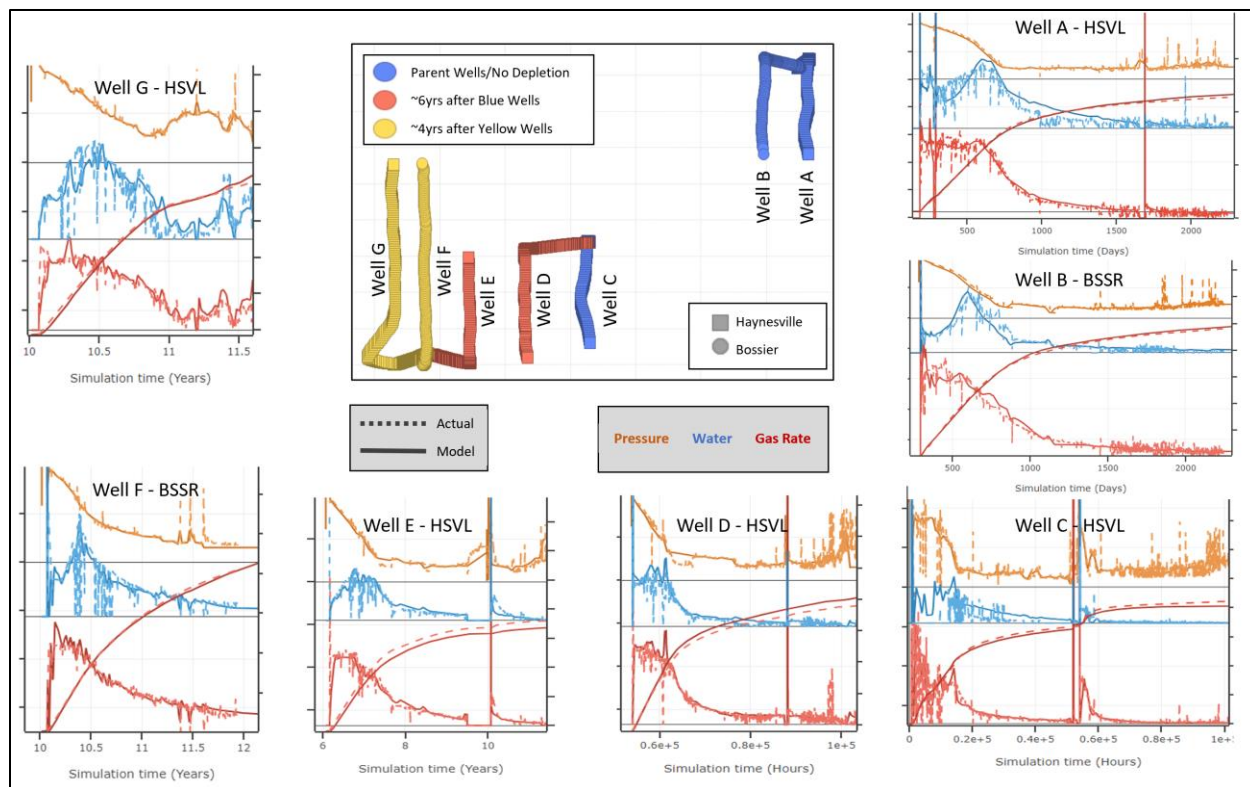
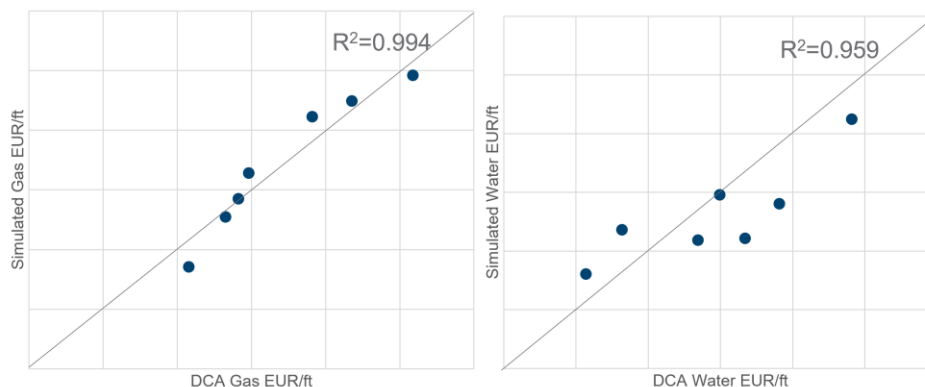Figure 18. Final production history matches for 7 wells in core study area

Figure 19. Comparison between model EUR predictions and decline curve-derived EURs

3. Model Validation and Sensitivities

The calibrated model parameters were employed to investigate a variety of design sensitivities. Design sensitivities were conducted for Haynesville and Bossier intervals on cluster spacing, stage length, well spacing, proppant loading, fluid loading, landing zone, and limited entry. Also tested were various development scenarios exploring inter-bench and intra-bench depletion under varying well spacings, well ages, parent designs, and child designs. While a deep review of these results is out of scope for this paper, an example of a model validation while reviewing field data warrants discussion.

Recent efforts in field data surveillance had aggregated ISIPs for several wells with varying cluster spacings. This field data observed an aggregate of 100 psi increase in ISIPs when tightening cluster

spacing from 20ft to 10ft. As is shown in **Figure 20**, a sensitivity analysis on cluster spacing from a base case Haynesville well design predicts a similar ISIP trend. Given that these wells were not part of the data used to calibrate this model, greater confidence in the predictivity of this parameter set was developed.
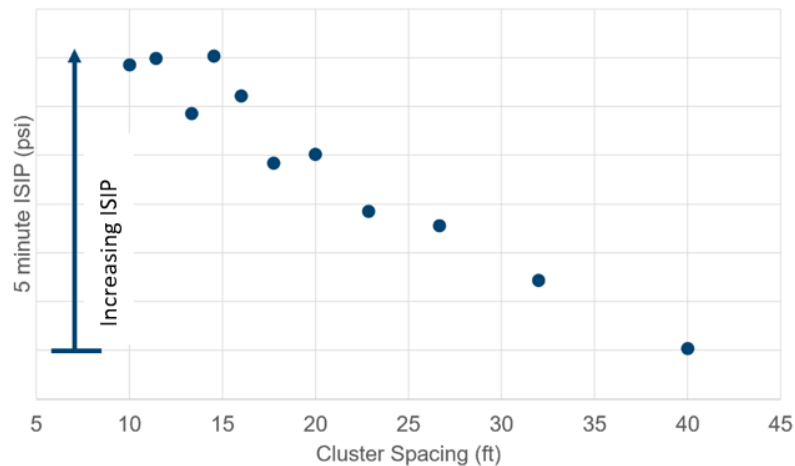

Figure 20. Model ISIPs for different cluster spacings

4. Conclusions

A numerical simulation generating a history match of rates and pressures may be one of thousands of non-unique solutions. Calibration points applied to frac geometry and reservoir depletion are critical to increasing the uniqueness of the solution and improving confidence in the model. Data from laboratory and field diagnostic tests in the representative area can be applied to refine the range of potential outcomes for each "tuning parameter" within the model. While examining each diagnostic individually may yield a broad spectrum of possible outcomes, integrating multiple diagnostics allows a continual narrowing toward a more definitive solution. This paper reviewed the framework for the application of traditional calibration techniques and introduced the utilization of additional tailored calibrations for increased accuracy. The approach to bolster model confidence encompasses the following steps:

1. **Base Stress Profile** – Incorporated eleven toe DFITs in multiple landing zones to calibrate the vertical stress profile
2. Utilized stimulation data such as ISIP observations to determine stress shadow effects
3. Initial History Match – Phase 1: Parent wells
4. Pressure Dependent Permeability and Embedment Laboratory Data – Utilized lab data to generate ranges of model input parameters
5. **Phase 2: Time-Lapse DQI testing** – This testing substantially narrowed the range of feasible solutions. This particularly supported the calibration of embedment and pressure-dependent permeability inputs, which were found to be the primary driver of reduced conductivity as reservoir pressure decreases.
6. **Darkvision – Post Job Perforation Analysis -** Correlated cluster-to-cluster stress shadow effects to cluster efficiency based on a number of parameters including limited entry and cluster spacing
7. **Final History Match – Phase 3: Child Wells –** Using model inputs from above, history matched additional wells including various development styles, completion vintages, and depletion conditions from offsets (parent/child effects)
8. Empirical Frac Gradient / ISIP - Ran sensitivities on completion to generate modeled ISIP output, cross-checked with field observations correlated to Cluster spacing, and Co-Development

While all of the above were included in the study, parameters of significant impact to the project are in bold.

The application of a robust set of DFIT data points in multiple horizons effectively provided a vertical stress profile in the zone of interest, thereby increasing confidence in the predicted frac growth. In addition, time-lapse interference testing was incorporated as a model constraint. While interference testing is not believed to be solely sufficient to describe fracture interaction, as it lacks a description of the number or location of connections, this data provided crucial information relating to fracture conductivity changes over time/pressure depletion. Incorporation of this data supported the separation of fracture conductivity loss caused by mechanisms such as proppant embedment from reservoir effects such as pressure-dependent permeability. Finally, post-frac perforation analysis combined with history matching of ten wells with variable completion vintages, spacing, parent/child developments, and co-development of multiple horizons increased confidence that a sufficiently unique solution had been achieved. The resulting set of modeling parameters was well-constrained and increased confidence in the model's accurate representation of the investigated area.

This paper provided a comprehensive examination of the history matching process in a physics-based numerical model, highlighting its value through the integration of various data types to corroborate observations across multiple types of analyses. The study facilitated an enhanced understanding of how predictive modeling can be strategically applied to optimize numerous variables, such as drawdown strategies, completion optimization, spacing, and co-development/targeting scenarios. The development of a model with high confidence levels presents compelling evidence that supports the implementation of testing scenarios for the future advancement of Chesapeake Energy.

Acknowledgments

References

Almasoodi, M., Andrews, T., Johnston, C., et al. 2023. A New Method for Interpreting Well-to-Well Interference Tests and Quantifying the Magnitude of Production Impact: Theory and Applications in a Multi-Basin Case Study. ArXiv [Physics.Geo-Ph]. arXiv. https://doi.org/10.48550/arXiv.2302.01968

Belyadi, H., Yuyi, S., and Junca-Laplace, J. 2015. Production Analysis Using Rate Transient Analysis. Paper presented at the SPE Eastern Regional Meeting, Morgantown, West Virginia, USA, October 2015. SPE-177293-MS. https://doi.org/10.2118/177293-ms

Blanton, T. L., and J. E. Olson. 1999. Stress Magnitudes from Logs: Effects of Tectonic Strains and Temperature. *SPE Reservoir Evaluation & Engineering* **2** (01): 62–68. https://doi.org/10.2118/54653-pa

Cipolla, C. L., Warpinski, N. R., Mayerhofer, M. J. et al. 2008. The Relationship between Fracture Complexity, Reservoir Properties, and Fracture Treatment Design. Paper presented at the SPE Annual Technical Conference and Exhibition, Denver, Colorado, USA, September 2008. SPE-115769-MS. https://doi.org/10.2118/115769-MS

Dontsov, E. V. 2022. A Continuous Fracture Front Tracking Algorithm with Multi Layer Tip Elements (MuLTipEl) for a Plane Strain Hydraulic Fracture. *Journal of Petroleum Science & Engineering* **217**: 110841. https://doi.org/10.1016/j.petrol.2022.110841

EIA. 2022. Proved Reserves of Crude Oil and Natural Gas in the United States, Year-End 2021. U.S. Energy Information Administration. https://www.eia.gov/naturalgas/crudeoilreserves/ (accessed 10 March 2024)

Fowler, G., McClure, M., and Allen, J. 2020. RTA Assisted History Matching with a Combined Hydraulic Fracturing and Reservoir Simulator. Paper presented at the SPE Latin American and Caribbean Petroleum Engineering Conference, Virtual, July 2020. SPE-199149-MS. https://doi.org/10.2118/199149-ms

Fowler, G., Jose, G., Jones, D. et al. 2023. A Success Story: Screening and Optimizing Refracs in the Eagle Ford. Paper presented at the SPE/AAPG/SEG Unconventional Resources Technology Conference, Denver, Colorado, USA, June 2023. URTEC-3848875-MS. https://doi.org/10.15530/urtec-2023-3848875

Hammes, U., Hamlin, H.S., and Ewing, T.E. 2011. Geologic Analysis of the Upper Jurassic Haynesville Shale in East Texas and West Louisiana. *AAPG Bulletin* **95** (10): 1643–66. https://doi.org/10.1306/02141110128

Heller, R., Vermylen, J., and Zoback, M. 2014. Experimental Investigation of Matrix Permeability of Gas Shales. *AAPG Bulletin* **98** (5): 975–95. https://doi.org/10.1306/09231313023

Jha, H. S., and Lee, W.J. 2017. Problems with Application of Material Balance Time to Transient Flow Data in Diagnostic Plots. Paper presented at the SPE/AAPG/SEG Unconventional Resources Technology Conference, Austin, Texas, USA, July 2017. URTEC-2697627-MS. https://doi.org/10.15530/urtec-2017-2697627

King, G. E., Rainbolt, M.F., and Swanson, C. 2017. Frac Hit Induced Production Losses: Evaluating Root Causes, Damage Location, Possible Prevention Methods and Success of Remedial Treatments. Paper presented at the SPE Annual Technical Conference and Exhibition, San Antonio, Texas, USA, October 2017. SPE-187192-MS. https://doi.org/10.2118/187192-ms

McClure, M., Bammidi, V., Cipolla, C. et al. 2019. A Collaborative Study on DFIT Interpretation: Integrating Modeling, Field Data, and Analytical Techniques. Paper presented at the SPE/AAPG/SEG Unconventional Resources Technology Conference, Denver, Colorado, USA, July 2019. URTEC-2019-123-MS. https://doi.org/10.15530/urtec-2019-123

McClure, M., Fowler, G., Hewson, C. et al. 2022. The A to Z Guide to Accelerating Continuous Improvement with ResFrac. ArXiv [Physics.Geo-Ph]. arXiv. https://doi.org/10.48550/arXiv.2205.14820

McClure, M., Fowler, G., Picone, M. 2022. Best Practices in DFIT Interpretation: Comparative Analysis of 62 DFITs from Nine Different Shale Plays. Paper presented at the SPE International Hydraulic Fracturing Technology Conference & Exhibition, Muscat, Oman, January 2022. SPE-205297-MS. https://doi.org/10.2118/205297-ms

McClure, M., Kang, C., Medam, S. et al. 2023. ResFrac Technical Writeup. ArXiv [Physics.Geo-Ph]. arXiv. http://arxiv.org/abs/1804.02092v15

Parker, M., Buller, D., Petre, E. et al. 2009. Haynesville Shale-Petrophysical Evaluation. Paper presented at the SPE Rocky Mountain Petroleum Technology Conference, Denver, Colorado, April 2009. SPE-122937-MS. https://doi.org/10.2118/122937-ms

Pearson, C. M., and Fowler, G. 2022. The Impact of Extended-Time Proppant Conductivity Impairment on the Ultimate Recovery from Unconventional Horizontal Well Completions. Paper presented at the SPE International Hydraulic Fracturing Technology Conference & Exhibition, Muscat, Oman, January 2022. SPE-205294-MS. https://doi.org/10.2118/205294-ms

Pudugramam, S., Irvin, R., McClure, M. et al. 2022. Optimizing Well Spacing and Completion Design Using Simulation Models Calibrated to the Hydraulic Fracture Test Site 2 (HFTS-2) Dataset. Paper presented at the SPE/AAPG/SEG Unconventional Resources Technology Conference, Houston, Texas, USA, June 2022. URTEC-3723620-MS. https://doi.org/10.15530/urtec-2022-3723620.

Ratcliff, D., McClure, M., Fowler, G., et al. 2022. Modelling of Parent Child Well Interactions. Paper presented at the SPE Hydraulic Fracturing Technology Conference and Exhibition, The Woodlands, Texas, USA, February 2022. SPE-209152-MS. https://doi.org/10.2118/209152-MS

Singh, A. and Zoback, M. 2022. Predicting Variations of the Least Principal Stress with Depth: Application to Unconventional Oil and Gas Reservoirs Using a Log-Based Viscoelastic Stress Relaxation Model. *Geophysics 87* (3): MR105–MR116. https://doi.org/10.1190/geo2021-0429.1

Singh, A., Zoback, M., and McClure, M. 2020. "Optimization of Multi-Stage Hydraulic Fracturing in Unconventional Reservoirs in the Context of Stress Variations with Depth." Paper presented at the SPE Annual Technical Conference and Exhibition, Virtual, October 2020. SPE-201739-MS. https://doi.org/10.2118/201739-ms

Thiercelin, M. J., and R. A. Plumb. (1994) Core-Based Prediction of Lithologic Stress Contrasts in East Texas Formations. *SPE Form Eval 9* (04): 251–258. SPE-21847-PA. https://doi.org/10.2118/21847-PA

Thompson, J. W., Fan, L., Grant, D. et al. 2010. An Overview of Horizontal Well Completions in the Haynesville Shale. Paper presented at the Canadian Unconventional Resources and International Petroleum Conference, Calgary, Alberta, Canada, October 2010. SPE-136875-MS. https://doi.org/10.2118/136875-ms

Torsch, W. C. 2012. *Thermal and Pore Pressure History of the Haynesville Shale in North Louisiana: A Numerical Study of Hydrocarbon Generation, Overpressure, and Natural Hydraulic Fractures.* Master's Thesis, Louisiana State University, Baton Rouge, Louisianna, USA (2012) https://doi.org/10.31390/gradschool_theses.268

Younes, Amgad I., H. Moore, N. Suurmeyer, Paul R. Smith, and M. Sandstrom. 2011. Development of Mechanically Layered Haynesville-Bossier Shale-Gas Play. Oral presentation given at the AAPG Annual Convention and Exhibition, Houston, Texas, USA, April 10-13, 2011.